INVESTIGATION OF FRACTURE RESISTANCE IN MICROSTRUCTURES OF INTERMETALLIC MATERIALS FOR HIGH TEMPERATURE SERVICE

By

David L. Davidson
Kwai S. Chan
James Lankford

AFOSR ANNUAL REPORT

This research was sponsored by the Air Force Office of Scientific Research,
Directorate of Chemistry and Materials Science
Under Contract F49620-92-C-0022
Approved for release; distribution unlimited

March 31, 1993

SOUTHWEST RESEARCH INSTITUTE
SAN ANTONIO HOUSTON
DETROIT WASHINGTON, DC

INVESTIGATION OF FRACTURE RESISTANCE IN MICROSTRUCTURES OF INTERMETALLIC MATERIALS FOR HIGH TEMPERATURE SERVICE

By
David L. Davidson
Kwai S. Chan
James Lankford

AFOSR ANNUAL REPORT

SwRI Project No. 06-4915
Contract No. F49620-92-C-0022

March 31, 1993

APPROVED:

Gerald R. Leverant, Director
Materials and Mechanics
Department

The Contractor, Southwest Research Institute, hereby certifies that, to the best of its knowledge and belief, the technical data delivered herewith under Contract No. F49620-92-C-0022 is complete, accurate, and complies with all requirements of the contract.

4/8/93
Date

Ulric S. Lindholm, Vice President
Engineering and Materials Sciences Division

SOUTHWEST RESEARCH INSTITUTE
SAN ANTONIO, TEXAS • HOUSTON, TEXAS • DETROIT, MICHIGAN • WASHINGTON, DC

ASIAC 12567

REPORT DOCUMENTATION PAGE

Form Approved
OMB No. 0704-0188

1. AGENCY USE ONLY (Leave blank)	2. REPORT DATE	3. REPORT TYPE AND DATES COVERED
	March 31, 1993	Annual Report: 1 March 1992 - 31 March 93

4. TITLE AND SUBTITLE

Investigation of Fracture Resistance in Microstructures of Intermetallic Materials for High Temperature Service

5. FUNDING NUMBERS

61102F 2306 AS

6. AUTHOR(S)

David L. Davidson, Kwai S. Chan, James Lankford

7. PERFORMING ORGANIZATION NAME(S) AND ADDRESS(ES)

Southwest Research Institute
6220 Culebra Road
San Antonio, TX 78238-5166

8. PERFORMING ORGANIZATION REPORT NUMBER

9. SPONSORING/MONITORING AGENCY NAME(S) AND ADDRESS(ES)

AFOSR/NE
Building 410, Bolling AFB DC
20332-6448

10. SPONSORING/MONITORING AGENCY REPORT NUMBER

F49620-92-C-0022

11. SUPPLEMENTARY NOTES

12a. DISTRIBUTION/AVAILABILITY STATEMENT

APPROVED FOR PUBLIC RELEASE; DISTRIBUTION IS UNLIMITED.

12b. DISTRIBUTION CODE

13. ABSTRACT *(Maximum 200 words)*

Smooth specimens of a fully lamellar TiAl-based alloy were cycled in reverse bending in order to study the initiation and growth of fatigue cracks. Cyclic deformation prior to crack initiation was studied with Atomic Force Microscopy. Deformation was found to occur mainly within the boundary region between lamellae, with strains as high as 50%, but fatigue cracks did not form in these boundaies. The slope of the stress-lifetime curve was ≈ 0.17. Stresses within ≈15% of ultimate stress were required to cause fracture in several million cycles. Small fatigue cracks formed within peculiar looking regions of microstructure where the lamellae were curved. These cracks would not continue to grow unless the stress amplitude was stepped up with contined cycling. A "small crack effect" was identified.

Other deformation and fracture characteristics of the TiAl-based alloy recently identified include the strain rate sensitivity of the tensile ductility, which is governed by the size of the colonies of lamellae, and the strain rate insensitivity of the fracture toughness at 25°C. However, at 800°C, fracture toughness is rate sensitive. The relative high fracture toughness of these alloys has been found to arise from a resistance curve behavior caused from ligaments that form behind the tearing crack tip. These ligaments result from the non-coplanar nature of microcracks that form during crack growth.

Composites of Nb-Cr alloys formed *in situ* showed fracture toughness values up to ≈ 8 MPa$\sqrt{m}$, which is ≈ 4X better than Cr_2Nb. Fatigue crack growth rate slopes for two composites were in the range of 20 to 70. Further work on these composites is in progress.

14. SUBJECT TERMS			15. NUMBER OF PAGES
			16. PRICE CODE
17. SECURITY CLASSIFICATION OF REPORT	18. SECURITY CLASSIFICATION OF THIS PAGE	19. SECURITY CLASSIFICATION OF ABSTRACT	20. LIMITATION OF ABSTRACT
UNCLASSIFIED	UNCLASSIFIED	UNCLASSIFIED	

GENERAL INSTRUCTIONS FOR COMPLETING SF 298

The Report Documentation Page (RDP) is used in announcing and cataloging reports. It is important that this information be consistent with the rest of the report, particularly the cover and title page. Instructions for filling in each block of the form follow. It is important to ***stay within the lines*** to meet ***optical scanning requirements***.

Block 1. Agency Use Only *(Leave blank)*.

Block 2. Report Date. Full publication date including day, month, and year, if available (e.g. 1 Jan 88). Must cite at least the year.

Block 3. Type of Report and Dates Covered. State whether report is interim, final, etc. If applicable, enter inclusive report dates (e.g. 10 Jun 87 - 30 Jun 88).

Block 4. Title and Subtitle. A title is taken from the part of the report that provides the most meaningful and complete information. When a report is prepared in more than one volume, repeat the primary title, add volume number, and include subtitle for the specific volume. On classified documents enter the title classification in parentheses.

Block 5. Funding Numbers. To include contract and grant numbers; may include program element number(s), project number(s), task number(s), and work unit number(s). Use the following labels:

C	- Contract	**PR**	- Project
G	- Grant	**TA**	- Task
PE	- Program Element	**WU**	- Work Unit Accession No.

Block 6. Author(s). Name(s) of person(s) responsible for writing the report, performing the research, or credited with the content of the report. If editor or compiler, this should follow the name(s).

Block 7. Performing Organization Name(s) and Address(es). Self-explanatory.

Block 8. Performing Organization Report Number. Enter the unique alphanumeric report number(s) assigned by the organization performing the report.

Block 9. Sponsoring/Monitoring Agency Name(s) and Address(es). Self-explanatory.

Block 10. Sponsoring/Monitoring Agency Report Number. *(If known)*

Block 11. Supplementary Notes. Enter information not included elsewhere such as: Prepared in cooperation with...; Trans. of...; To be published in.... When a report is revised, include a statement whether the new report supersedes or supplements the older report.

Block 12a. Distribution/Availability Statement. Denotes public availability or limitations. Cite any availability to the public. Enter additional limitations or special markings in all capitals (e.g. NOFORN, REL, ITAR).

- **DOD** - See DoDD 5230.24, "Distribution Statements on Technical Documents."
- **DOE** - See authorities.
- **NASA** - See Handbook NHB 2200.2.
- **NTIS** - Leave blank.

Block 12b. Distribution Code.

- **DOD** - Leave blank.
- **DOE** - Enter DOE distribution categories from the Standard Distribution for Unclassified Scientific and Technical Reports.
- **NASA** - Leave blank.
- **NTIS** - Leave blank.

Block 13. Abstract. Include a brief *(Maximum 200 words)* factual summary of the most significant information contained in the report.

Block 14. Subject Terms. Keywords or phrases identifying major subjects in the report.

Block 15. Number of Pages. Enter the total number of pages.

Block 16. Price Code. Enter appropriate price code *(NTIS only)*.

Blocks 17. - 19. Security Classifications. Self-explanatory. Enter U.S. Security Classification in accordance with U.S. Security Regulations (i.e., UNCLASSIFIED). If form contains classified information, stamp classification on the top and bottom of the page.

Block 20. Limitation of Abstract. This block must be completed to assign a limitation to the abstract. Enter either UL (unlimited) or SAR (same as report). An entry in this block is necessary if the abstract is to be limited. If blank, the abstract is assumed to be unlimited.

EXECUTIVE SUMMARY

Substantial progress has been made in understanding the deformation and fracture properties of fully lamellar TiAl-based alloys, particularly fatigue crack initiation characteristics. Work was also initiated during this past contract year on studying the deformation and fracture characteristics of a series of *in-situ* formed composites formed from the niobium and chromium binary system.

Smooth specimens of a fully lamellar TiAl-based alloy were cycled in reverse bending in order to study the initiation and growth of fatigue cracks. The development of cyclic deformation observed prior to crack initiation was studied with replication and the scanning probe microscopies, particularly Atomic Force Microscopy (AFM), which is capable of atomic resolution measurements of surface topography. For practical use of this new microscopy technique on specimens of constructional meterials of interest to the Air Force, the technique of making AFM measurements from replicas was developed. Thus, specimens of complex shapes not otherwise adaptable to these probe instruments can be examined. The capabilites of this new technique are sufficient to allow measurements useful to the understanding of cyclic deformation; the limitations of this technique are still being explored.

Cyclic deformation was found to occur mainly within the boundary region between lamellae, although some deformation within lamellae cannot be excluded. Strains as high as 50% were measured in some boundaries, but this level of damage concentration did not lead to the formation of fatigue cracks. The slope of the stress-lifetime curve was very shallow, having a slope of approximately 0.17, which means that stresses well in excess of yield and within $\approx$ 15% of ultimate stress are required to cause fracture in several million cycles. This value was as anticipated from the slope of the fatigue crack growth rate curve previously measured for this alloy. The outstanding fatigue crack initiation resistance found for this alloy is rare for materials with engineering potential.

When fatigue cracks did form in this alloy, it was found that they occurred within peculiar looking regions of microstructure where the otherwise straight lamellae were curved. Further evidence of the outstanding fatigue crack resistance of this material was indicated when it was found that these cracks would not continue to grow unless the stress amplitude was stepped up with continued cycling. This would indicate that the fatigue limit in this material is set by the growth of small cracks, not by the initiation of cracks. The growth of small cracks was measured, and "a small crack effect" was identified; i.e., small cracks grew at values of cyclic stress intensity factor lower than would be possible for large fatigue cracks.

Other deformation and fracture characteristics of the TiAl-based alloy recently identified include the strain rate sensitivity of the tensile ductility, which is governed by the size of the colonies of lamellae, and the strain rate insensitivity of the fracture toughness at 25°C. However, at 800°C, fracture toughness is rate sensitive.

The relative high fracture toughness of these alloys has been found to arise from a resistance curve behavior caused from ligaments that form behind the tearing crack tip. These ligaments result from the non-coplanar nature of microcracks that form during crack growth. Redundant deformation and fracture within the ligaments leads to a toughening behavior that is similar to ductile phase toughening.

The *in situ* composites formed from Nb-Cr alloys showed fracture toughness values up to $\approx$ 8 MPa$\sqrt{m}$, which is up to a factor of 4 better than the toughness of the intermetallic compound Cr_2Nb. Fatigue crack growth rates were measured for two composites and the slopes of the curves were found to be in the range of 20 to 70, i.e., a factor of at least 10 greater than found for other titanium alloys, including the TiAl-based materials. Further work on these composites is in progress.

PERSONNEL

PERSONNEL

The following personnel obtained partial support from this contract during the past year:

Principal Investigators: Drs. D. L. Davidson, K. S. Chan, and J. Lankford

Technical Support: Dr. Y-M. Pan, J. B. Campbell, B. K. Chapa, H. E. Saldana, and J. F. Spencer.

ATOMIC FORCE MICROSCOPY OF SURFACE REPLICAS

ATOMIC FORCE MICROSCOPY OF SURFACE REPLICAS

Because of the nature of the titanium-aluminides, conventional imaging modes (especially SEM) for assessing mechanisms of plastic flow and damage are relatively unenlightening. The relevant details are extremely fine scale, and produce little scanning electron contrast. It has therefore become necessary to turn to an alternative approach, namely, atomic probe microscopy. Unfortunately, this technique has its own limitations, principally connected with its highly constrained physical motion relative to a sample, and to the physical nature of the samples which can be accommodated by an atomic probe device.

In order to appreciate these limitations, it is necessary to consider the nature of the technological questions at the heart of our research. Specifically, we must characterize: (1) the details of crack nucleation within cyclic plasticity-induced slip bands or damage zones; (2) fine-scale fracture surface features; (3) crack-tip opening and incremental crack extension micromechanisms. In regard to issues (1) and (3), it is virtually impossible to position an atomic force or scanning tunneling microscope on the actual specimen and thereby generate images of the desired surface features. In regard to issue (2), fracture surfaces are so irregular that it generally is impossible to orient a particular small region nearly normal to the Z-axis of the tip, as is required for effective imaging.

A possible means of defeating this problem is the use of plastic replicas of the desired areas, since they can easily be sized and manipulated to accommodate the requirements of the atomic probe apparatus. In fact, recent atomic force microscope (AFM) experiments described in the following section show that this approach does, indeed, provide valid, high resolution surface images of otherwise difficult or impossible to interrogate areas.

The relatively young technology (since 1986) of atomic force microscopy (AFM) already has been applied to high resolution imaging in many scientific disciplines.[1] Basically, a specimen is rastered by piezoelectric translation devices below an atomically sharp tip. The tip is mounted on a cantilever that functions as a highly sensitive spring. Initial contact occurs when the distance between the tip and sample is decreased to a point at which long range, attractive van der Waals forces pull the tip to within a few nanometers of the surface. Atomic repulsive and attractive forces on the tip are then in equilibrium, maintaining the tip at a height of a few nanometers. As the probe scans the surface, it responds to changes in surface height by reacting through the cantilever, thus allowing it to maintain the same surface-tip separation; i.e.; the tip deflects relative to its attachment point. The deflection is measured and processed with relation to the tip's x-y raster position, in turn, forming a topographic image of the scanned surface. AFM has recently been utilized to study deformation and fracture processes in engineering materials, although with serious limitations as noted above.

At first consideration, the proposed application of AFM to the examination of surface replicas may seem contradictory; one immediately questions the validity of the concept on the basis of the potential clouding of the intrinsic atomic resolution capability of the AFM by applying it to an object which must itself have lost detail on that scale. On the other hand, direct AFM imaging of engineering materials has shown that the smallest observable (certainly relevant) surface microstructures are at least an order of magnitude larger in size than typical inter-atomic spacings and well within the generally accepted (5 nm) resolution of the replica techniques. Indeed, very few, if any, engineering materials can be processed into meaningful specimens and subsequently prepared in such a manner as to display atomic-scale surface structure observable by

AFM.*[1] Further practical advantages are found in maintaining a replica history of specimens. Often, a specimen will be destroyed either by accident or as part of experimental procedures. If a replica history of the life of the specimen has been maintained, information representative of the response of the specimen to the experimental conditions to which it has been exposed is recorded for subsequent examination. Thus, important information is not lost upon changing experimental conditions or by the failure of the specimen.

Replicas have long been used in metallurgical and material science as a primary means of specimen surface data collection.[2] Fracture surfaces, fatigue crack tips, growing surface fatigue microcracks and specimen surfaces that have been exposed to creep damage are common examples of material damage development that have been characterized by the microscopic examination of replicas. Optical microscopy and scanning and transmission electron microscopy have been used to examine replicas; all suffer from varying degrees of limited resolution. A brief discussion of these limitations is helpful to understand the rationale for applying AFM to replica examination.

Diffraction limited resolution and poor depth of field place optical microscopy in the position of having the worst resolution. Scanning electron microscopy, though diffraction limited, has demonstrated resolution on the order of 3 to 5 nm under ideal conditions, imaging specimens with high atomic number and topography. In practice, most areas of interest for high resolution SEM imaging of replicas are areas of very low topography, such as those found between or on top of striation structures on fatigue fracture surfaces. In cases such as this, SEM resolution is low, as the secondary electrons excited from the topographic surface layer that must be processed to form an image become lost in the total signal generated from the deeper electron beam–specimen interaction volume. Resolution is further hampered by poor signal to noise ratio, since the electron beam column is optimized to produce the smallest possible electron probe diameter, which is necessary for high resolution imaging. Decreasing the probe size increases instrument resolution; however, the decrease also produces a resultant decrease in probe current, hence, a decrease in the excitation of information carrying signal. High resolution techniques such as low loss back scattered electron imaging can greatly increase SEM resolution capabilities. However, these techniques generally are cumbersome to employ and yield highly fore-shortened images of poorer resolution than is available with AFM.

Transmission electron microscopy offers resolution that approaches the resolution capabilities of an AFM. However, the replica images produced by the TEM are actually highlighted shadows of the actual features. They are foreshortened and distorted, and as for the SEM, require relatively steep height gradients in order to manifest contrast. Also, the generation of TEM replicas (metal shadowed, carbon film negatives of their plastic film "parent") is extremely labor intensive and therefore costly.

A potential problem of some concern in AFM replica imaging is that of sample vibration. Thus, mounting is performed by holding the replica by its overlaps, centering the region of interest over the center of an AFM mounting disc, and tacking the edges of the replica to the mounting media. This procedure avoids mechanical damage to the area to be imaged, but obviously does not tightly couple the replica to the mounting disc at the imaging area. This was of great initial concern as it was suspected that poor coupling might induce or aggravate replica vibration, deleteriously affecting resolution. Experimentation with several complex methods of mounting virgin replica segments to various substrates that were, in turn, mounted to AFM discs after replication was

1. *Nearly all images of atoms have been obtained from carefully prepared, usually cleaved or freshly exposed, low index atomic planes in simple materials like graphite and mica.

performed. Upon comparison of images obtained from these replicas to actual substrate images (Figures 1 and 2), no difference in image quality due to vibration was detected in scans approaching the limits of resolution, which for most of the materials examined, occurs at about a 150 nm scan size, which corresponds in the figures to a lateral magnification of about 600,000X.

Replicas may be examined directly by AFM. The imaging mechanism is derived from the deflection of the AFM tip by surface features as the tip is rastered across the specimen surface; no current flow between tip and sample is necessary for imaging, as is the case in scanning tunneling microscopy, nor is the specimen subject to high energy electron bombardment, requiring the specimen surface to be protective and conductive, as in the SEM and TEM examination. However, if a selected area of interest is to be found and subsequently placed under the AFM tip for imaging, a means to image the tip and specimen simultaneously must be employed. This is usually done by low power optical microscopy. It is necessary, therefore, to coat the specimen surface with some material to make it reflective and thus observable with optical microscopy.

Vacuum deposition of metals onto replicas is a standard technique of preparing replicas for examination by optical or SEM techniques. The structure of the metallic coating is usually well below the resolution limits of optical microscopes or SEM's; with coatings produced by sputtering systems being superior, the best produced by low energy deposition in an apparatus designed to isolate the specimen from the sputtering plasma and other sources of radiation damage.

The material to be sputtered should ideally form a fine-grained film of very low topography when deposited and should be inert when exposed to atmospheric oxidation and hydration reactions; it should also be of high atomic number and low surface resistivity to enable high resolution SEM examination. The film should be as thin as possible in order to avoid compromising surface detail. We have found iridium films produced in a state-of-the-art VCR apparatus to meet these criteria.

To date, we have applied the AFM replica technique to two of the three cases discussed earlier, *e.g.,* slip band crack nucleation and microfractography. Crack-tip replication/AFM imaging experiments are planned for the coming year. Experiments to compare the resolution of AFM and TEM replicas are also planned, using γ TiAl as the experimental material base.

An example of fatigue-induced surface slip band formation in TiAl is shown in Figure 3. This image was taken from a replica of the polished surface of a rotating beam fatigue specimen. Figure 4 is a microfractographic image from a replica of the fatigue fracture surface of a compact tension γ TiAl specimen. Crack growth in the photo was approximately vertical; periodic markings and numerous microscopic "dimples" can be seen.

References

1. D. Sarid, Scanning Force Microscopy with Applications to Electric, Magnetic, and Atomic Forces, Oxford University Press, 1991.

2. J. Lankford and J. G. Barbee, *Journal of Materials Science*, **9**, p. 1906, 1974.

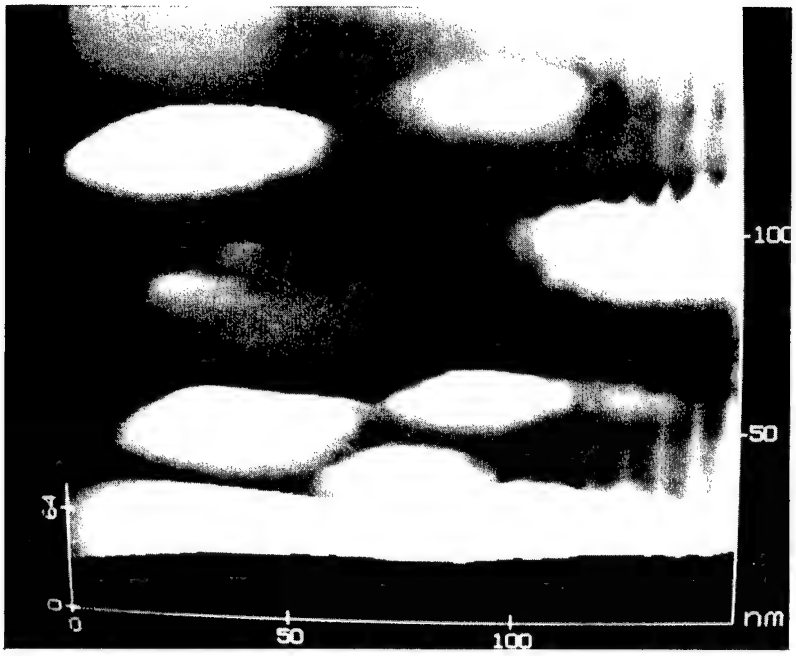

Figure 1. Atomic force image of ion-etched silicon, showing microstructural domains in relief.

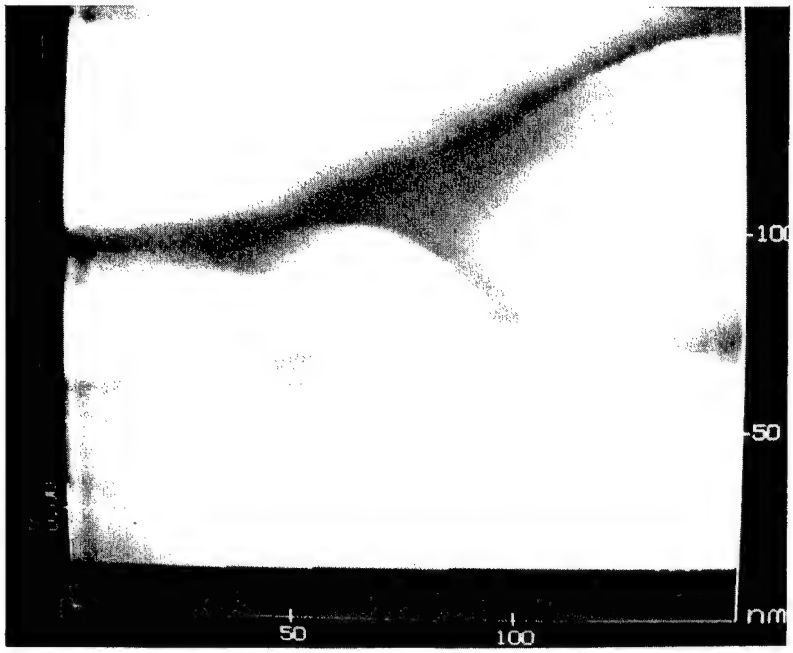

Figure 2. Atomic force image of iridium-coated plastic replica of substrate shown in Figure 1; similar features are visible.

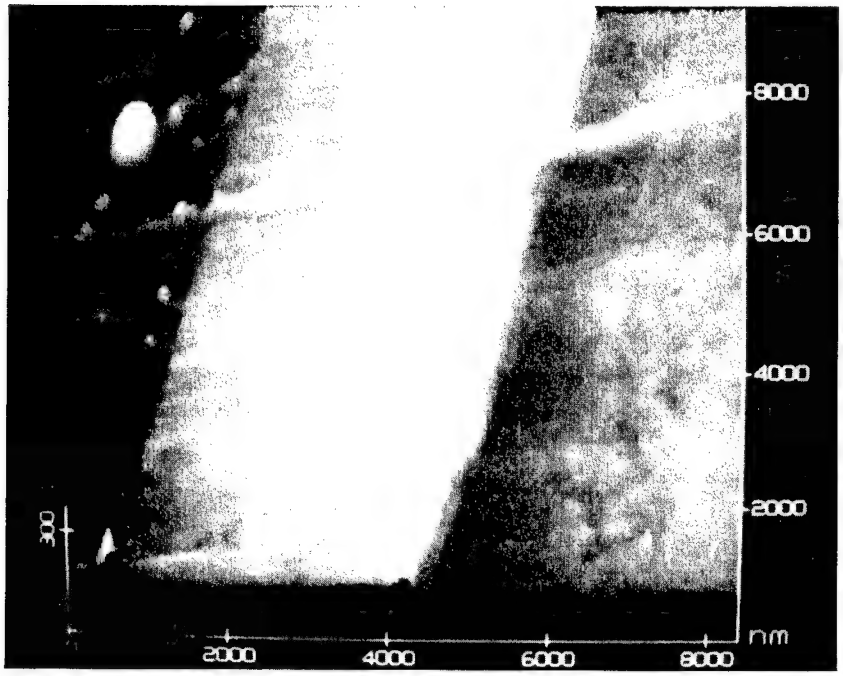

Figure 3. Atomic force image of fatigue-induced surface slip bands in TiAl; AFM sample consists of iridium-coated plastic replica.

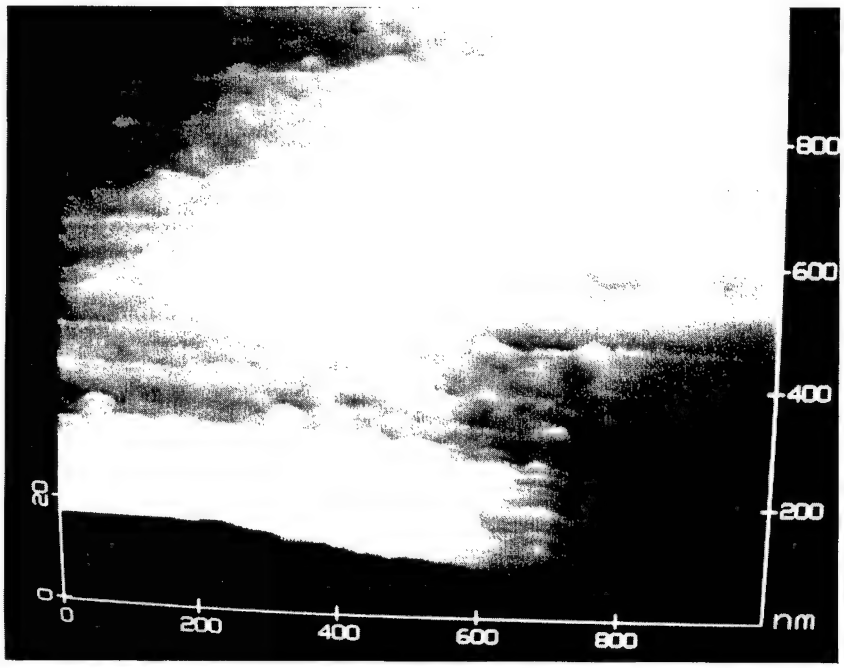

Figure 4. Atomic force image of fatigue fracture surface of TiAl; crack growth direction vertical.

FATIGUE AND FRACTURE IN LAMELLAR TiAl ALLOYS

FATIGUE AND FRACTURE IN LAMELLAR TiAl ALLOYS

Abstract

An overview of the fatigue and fracture mechanisms in lamellar TiAl alloys is presented. Investigations of tensile fracture, fatigue crack initiation, growth of small and large fatigue cracks, and fracture toughness properties are summarized. Pertinent crack-tip micromechanics measurements are utilized to illustrate the various processes by which a crack extends in lamellar TiAl alloys. Based on the results, the influence of microstructure, temperature, and when appropriate, loading rate on tensile properties, fatigue crack initiation and growth, and fracture toughness are elucidated and related to the controlling fracture mechanisms.

Introduction

Two-phase TiAl-base alloys can be heat-treated to exhibit a wide range of microstructures consisting various amounts of equiaxed gamma grains and lamellar colonies (1-3). In one extreme, the lamellar microstructure consists mostly, if not entirely, of colonies of aligned $\alpha_2 + \gamma$ platelets. In the other extreme, the equiaxed γ grain microstructure, as evident by the nomenclature, consists mostly of polygonal γ grains. In between the two extremes is the duplex microstructure, which is comprised of approximately equal volume fractions of lamellar colonies and equiaxed γ grains.

Recent studies (4-10) have shown that the fracture resistance of two-phase TiAl-alloys is sensitive to microstructure. For example, the lamellar microstructure has generally been found to exhibit a higher fracture toughness, but a lower tensile ductility than either the duplex or equiaxed γ microstructure. The fracture toughness exhibited by lamellar TiAl is in excess of 30 MPa$\sqrt{m}$ at ambient temperature. Most of this fracture toughness arises from the composite-like structure of the aligned $\alpha_2 + \gamma$ platelets in the lamellar microstructure. Recent fatigue studies (8-9,11-12) have also revealed that the lamellar microstructure plays an important role in the fatigue failure behavior of two-phase TiAl-alloys, with the range of effects spanning from cyclic deformation, fatigue crack initiation, to the growth of both small and large fatigue cracks.

This article presents an overview of our studies on the fatigue and fracture mechanisms in lamellar TiAl-alloys. The overview will highlight our findings of the important factors influencing the tensile ductility, cyclic deformation, fatigue crack initiation, the growth of small and large fatigue cracks, and fracture toughness behaviors of lamellar TiAl-alloys.

Experimental Procedures

The TiAl-base alloys utilized in our investigations were designated as G1L and G8L1, whose compositions are shown in Table 1. These materials were supplied by Dr. Young-Won Kim at Universal Energy Systems in the form of blocks cut from a forged pancake. The heat-treatment for the G1L material was 1340°C/1 hr $\rightarrow$ 900°C/6 hr/air cooled; it resulted in a nearly fully microstructure consisting of 95% lamellar colonies and 5% equiaxed gamma grains located at lamellar colony boundaries. The average colony size and lamellar spacing for G1L were 1200 μm and 1.8 μm, respectively. The heat-treatment for the G8L1 material was 1370°C/8 min./furnace cooled $\rightarrow$ 1000° C/air cooled, which resulted in a fully lamellar microstructure with 540 μm average colony size and 2.2 μm lamellar spacing. Figure 1 shows a micrograph of the fully lamellar microstructure of the G8L1 material.

Table 1 Chemical Composition of TiAl-Alloys Studied

	Composition								
	(in atomic %)					(in ppm by weight)			
Material	**Ti**	**Al**	**Nb**	**Cr**	**V**	**O**	**N**	**H**	**C**
G1L	Bal.	47	2.6	0.93	0.85	550	55	14	160
G8L1	Bal.	46.8	2.3	1.60	0.90	550	--	--	--

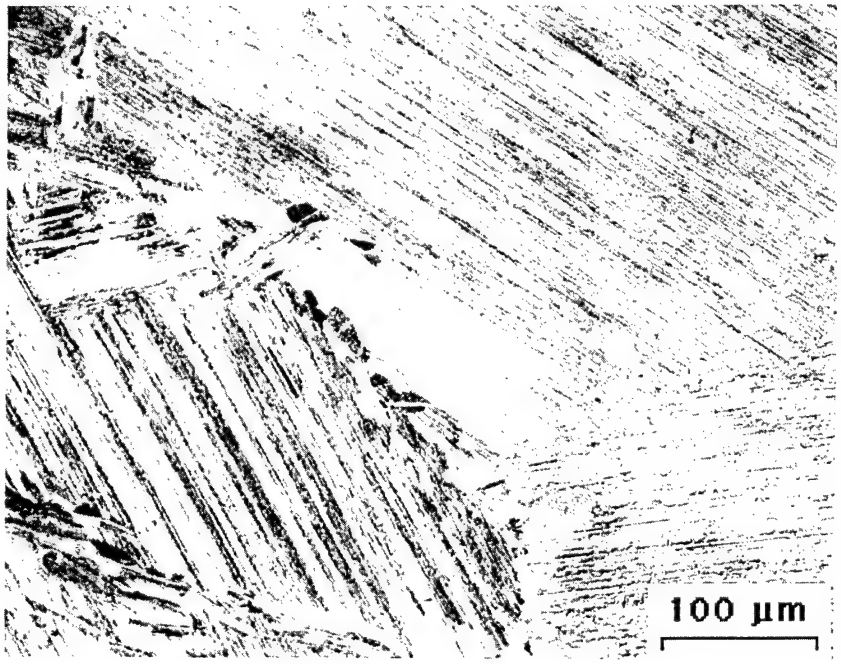

Figure 1: Typical microstructure of a fully lamellar TiAl-alloy (G8L1).

Tensile and fracture toughness tests were performed on the G1L materials. Both conventional and micromechanical testing were performed. The latter was conducted in a scanning electron micro-scope (SEM) equipped with a high-temperature loading stage. Details of the experimental procedures and specimen geometries are described elsewhere (4-5,13).

Fatigue crack initiation and growth studies have been carried out on a fully lamellar microstructure (G8L1 material). This work emphasized the detailed study of a few specimens rather than obtaining data for engineering use. The objective of the work was to identify the effects of microstructure and understand its effects on fatigue.

Fatigue crack initiation and the growth of small cracks ($2a < 100\ \mu m$) were studied using rotating beam specimens at 30 Hz under $R = -1$, where R is the ratio of the minimum to the maximum applied stress. Compact tension specimens were used to study the growth of large fatigue cracks. Plastic replicas were used to create a record of changes in the topography of the rotating beam specimens as the stress amplitude and number of cycles changed. Scanning electron microscopy (SEM) of the specimen surfaces and atomic force microscopy (AFM) of the replicas were used to study topographic changes.

Compact-tension specimens were cyclically loaded in a laboratory electrohydraulic frame at ambient temperature in air and at 800°C in a vacuum of $1x10^{-3}$ Pa. Cracks were initiated from a notch in compression-compression loading but grown using R = 0.1 and 10 Hz. Periodically these specimens were transferred to a cyclic loading stage that fitted within the specimen chamber of the SEM for observations and measurements of the crack-tip region under high resolution conditions at ambient temperature and 800°C (14). The stereoimaging technique (15) was used to make direct measurements of fatigue crack closure, and displacements were measured from the near crack tip region, using a machine-visioned based stereoimaging system, DISMAP (16), from photographs made within the SEM at minimum and maximum loads. Detailed observations of the growth of fatigue cracks were also made by loading within the SEM.

Results

Tensile Fracture

The tensile stress-strain behavior of the G1L alloy is sensitive to the imposed strain rate at both 25°C and 800°C. In general, an increase in strain rate leads to a slight increase in flow stress, but a large reduction in tensile ductility. Figure 2 shows comparison of the stress-strain curves for G1L tensile specimens tested at 800°C in air at strain rates of $1x10^{-3}$ and $1x10^{-5}$ sec^{-1} (13). The tensile ductility at the strain rate of $1x10^{-5}$ sec^{-1} is 9%, and it is reduced to 1% when the strain rate is increased to $1x10^{-3}$ sec^{-1}. This reduction in tensile ductility with increasing strain rate is the consequence of increasing propensity for flow localization at high strain rates.

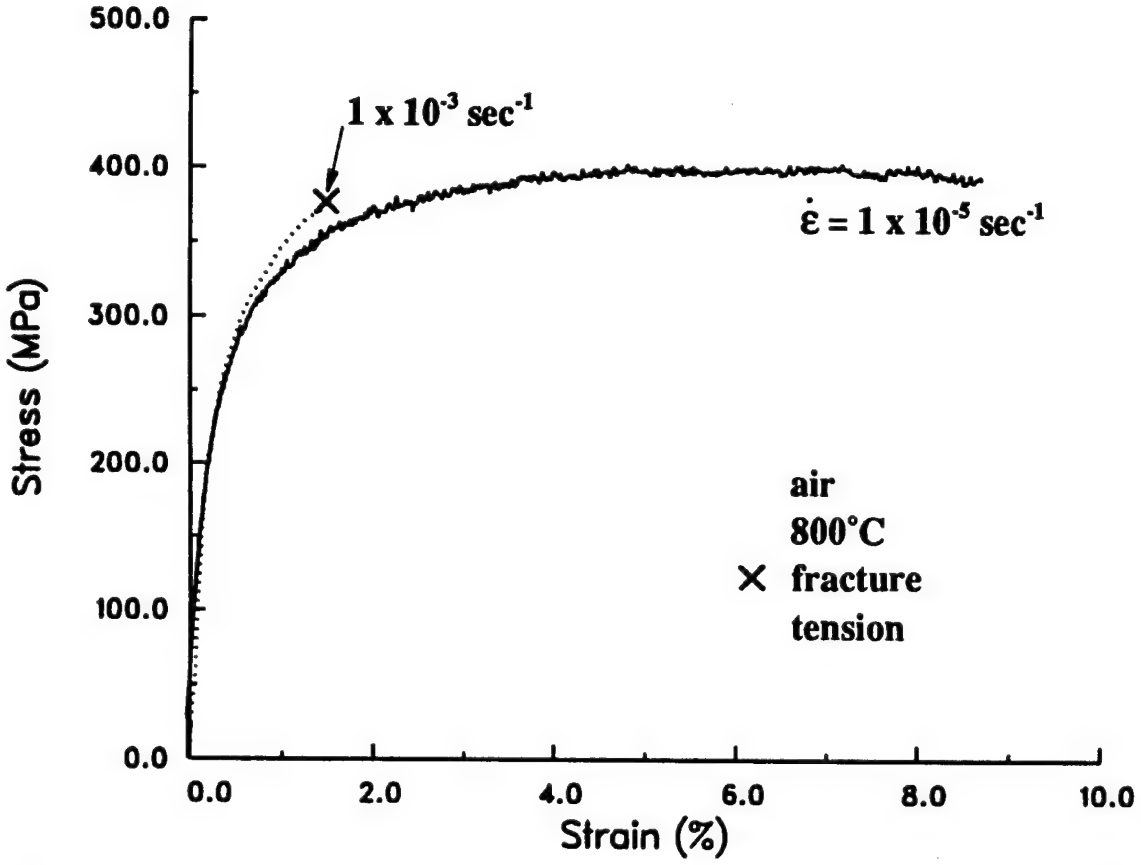

Figure 2: Comparison of the tensile stress-strain curves of the G1L alloy for two strain rates at 800°C in air.

Beside strain rate, the test environment also appears to influence the tensile stress-strain behavior of two-phase TiAl-alloys at 800°C at a slow strain rate ($1x10^{-5}$ sec^{-1}). In particular, the tensile specimen tested in SEM vacuum ($1x10^{-3}$ Pa) showed a higher flow stress, strain-hardening rate, and tensile ductility when compared to those in air or zero-grade argon. The tensile ductility of G1L observed at 800°C in vacuum is 29% for a strain rate of $1x10^{-5}$ sec^{-1}. The high ductility is, however, accompanied by the presence of numerous microcracks in the microstructure. This is illustrated in Figure 3 which shows initiation of microcracks in equiaxed γ grains located at lamellar colony boundaries at a strain as low as 3%. Upon increasing straining, the microcracks opened up but did not propagate. Instead, more microcracks were nucleated in both equiaxed γ grains and lamellar colonies. In all cases, the size of the microcracks was on the order of the size of microstructural unit where they were initiated, *i.e.*, the γ grain or the lamellar colony size. A large microcrack formed by separation of lamellar colony boundaries is shown in Figure 3. The large opening of the microcrack at a strain of 18% indicates that the observed tensile ductility arises from material's resistance to microcrack propagation. Additionally, opening of microcracks might have also inflated the measured value for tensile ductility.

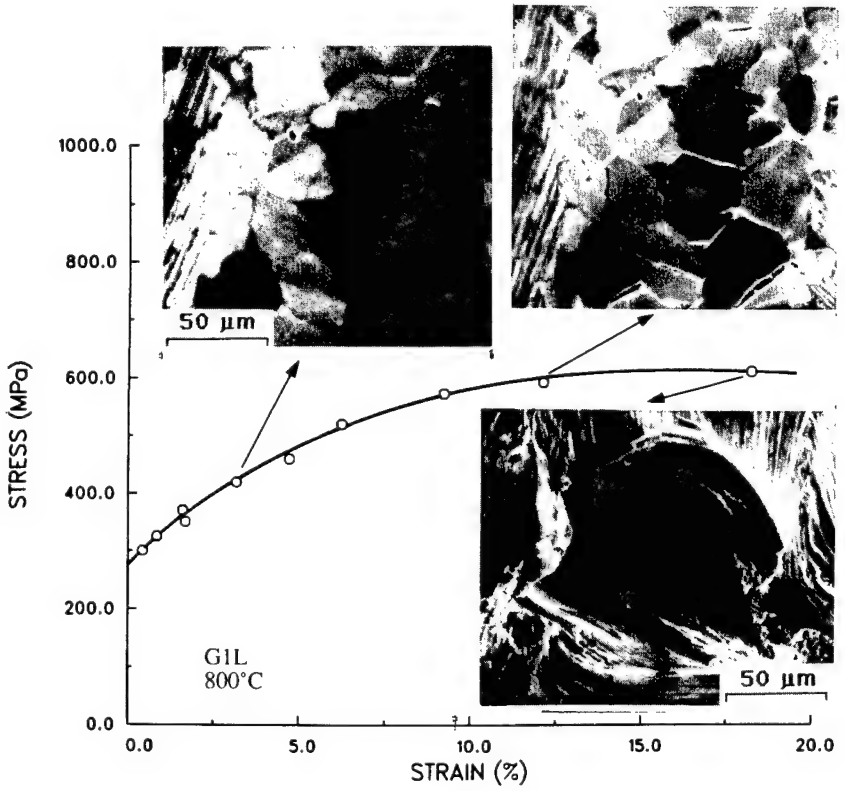

Figure 3. Formation of microcracks at equiaxed γ grains and lamellar colony boundaries in the G1L alloy during tensile deformation.

Cyclic Deformation and Fatigue Crack Initiation

The deformation and crack initiation characteristics of the lamellar G8L1 material are extraordinary. Only small amounts of deformation were detected below the macroscopic yield stress, and it was necessary to increase stress to far above yield to obtain fatigue crack initiation. As the material was cycled at a given stress level, deformation occurred between lamellae, leading to the development of a very rough microtopography. Almost all of the deformation was

out-of-plane shear; negligible amounts of in-plane deformation were detected. This behavior is opposite of that found for Astroloy (17) where in-plane shear was abundant and participated in the initiation of fatigue cracks.

An example of the deformation behavior found for this lamellar microstructure is shown by the AFM image of Figure 4. Below the AFM image is a topographic section taken across the image. From these sections, shear strains (gradients of displacements) as high as 50% were measured at the edges of wide lamellae or within regions of multiple narrow lamellae, indicating that very large strains could be sustained at some interlamellar regions without causing crack formation. At lower resolution, maximum strains averaging about 3% for a stress amplitude of 360 MPa were found. These strains may be compared with an elongation to fracture of 1.1% for the G8L1 alloy under monotonic tensile loading (3).

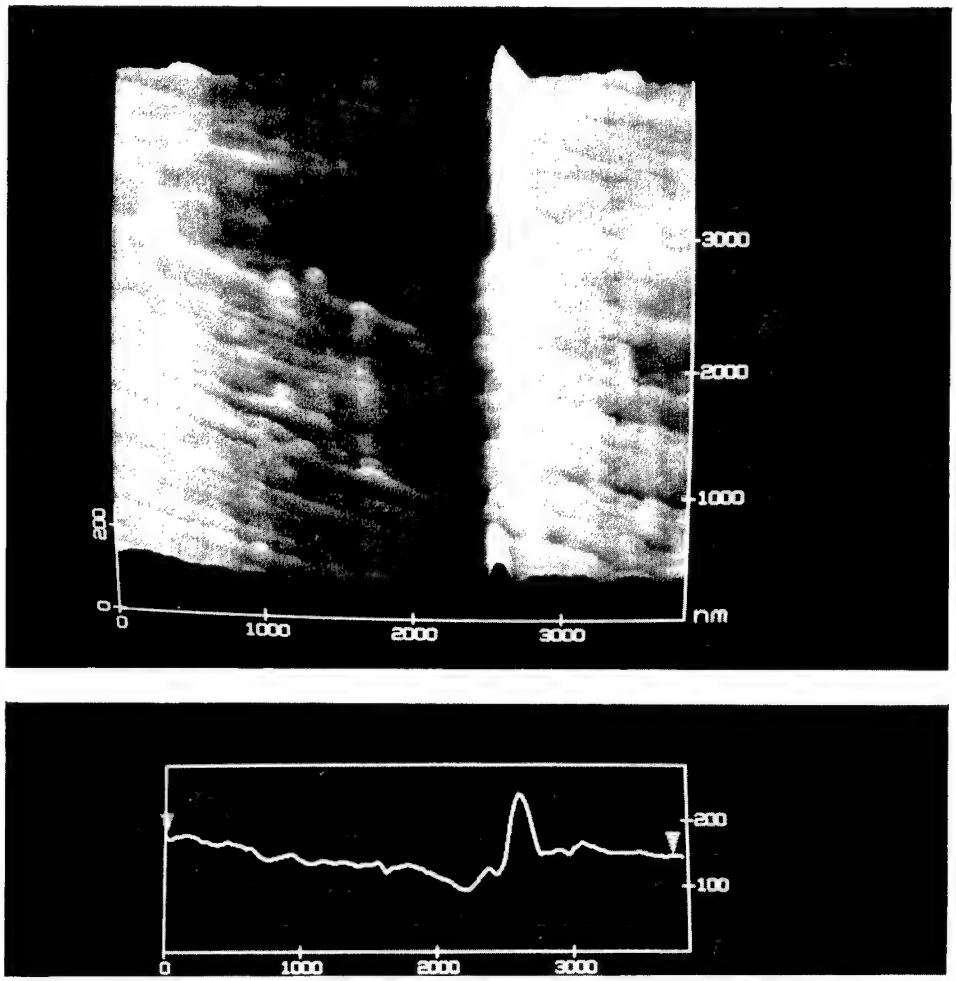

Figure 4. Atomic force microscopy of the lamellar microstructure loaded for $1x10^6$ cycles at a stress amplitude of 360 MPa. Upper image shows the topography across several of the lamellae and beneath it is a horizontal profile across center of the image. All dimensions shown are in nanometers.

For a given stress amplitude, the deformation that formed within the lamellae saturated, *i.e.*, continued cycling did not cause the strain amplitude to increase. Increasing the stress amplitude increased the extent of slip rather than the amplitude of strain within slipped regions. From

measurements of the extent of slip and its magnitude, such as shown in Figure 4, the cyclic stress-strain curve was derived, with a slope or cyclic hardening exponent, n′, of 0.17, which is about twice the cyclic work hardening rate usually found for aluminum alloys.

At 360 MPa, in one region of microstructure, two cracks about 30 μm were detected in an interlamellar region. The features observed were defined as cracks because they exhibited crack opening displacement (COD) when replicas of the specimen at minimum and maximum load were stereoimaged; however, these cracks did not grow on subsequent cycling and exhibited no COD, presumably due to the high work hardening coefficient of the material.

Fatigue cracks of sufficient size to grow did not initiate from the copious slip that formed during cycling. Instead, cracks initiated from microstructural defects that were found to exist prior to cycling, but only at a stress level well in excess of yield and over half the ultimate stress. The origin of these defects, found near the centers of colonies, where characterized as pockets of curved (or wavy) lamellae surrounded by straight lamellae. These pockets, one of which is shown in Figure 5, gave the impression of small deformed regions formed within a colony. They were rather like knots or burls often found in the microstructures of wood. Since forging was used in the processing of this microstructure, it is possible that these defects were forging related.

Figure 5. Unusual microstructural feature within a lamellar colony showing the site that initiated a fatigue crack.

Fatigue Crack Growth

The growth of small cracks initiated from these defects was intermittent and could not be sustained at the level of stress amplitude that initiated them. Cracks often stopped and remained dormant for extended periods (10^5 cycles), but crack growth could be induced again by applying a larger stress amplitude. The cracks, when small ($2a < 60$ μm), grew at a faster rate and at ΔK values below those found for large cracks. A direct comparison of crack growth rates is shown in Figure 6, although the comparison may not be appropriate because small cracks were grown at $R = -1$ at stress levels above yield while large cracks were grown at $R = 0.1$ under nominally elastic

loading. Large cracks cycled below $\Delta K \approx 4.5$ MPa$\sqrt{m}$ could not be induced to grow in $30x10^4$ cycles; thus, ΔK_{th} was estimated to be ≈ 4.2 MPa$\sqrt{m}$. Direct measurements of closure supported this estimate.

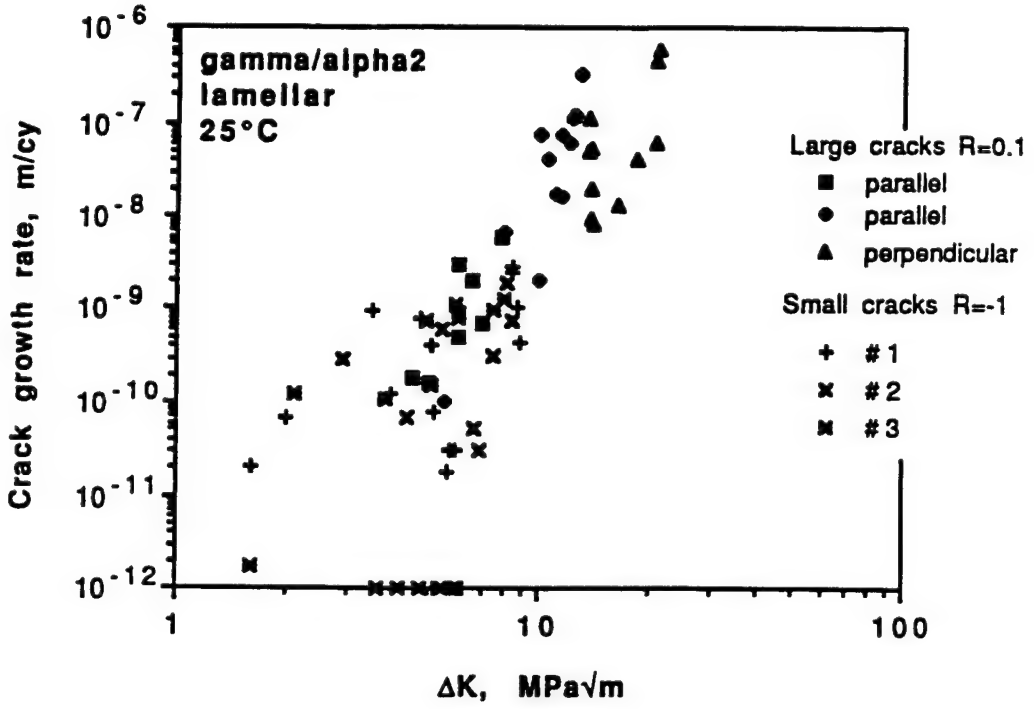

Figure 6. Crack growth rates for small and large cracks in the fully lamellar microstructure.

Deformation measured at the tips of fatigue cracks was dependent on the level of ΔK; crack-tip strains of up to 30% were found at ambient temperature, while at 800°C, maximum crack-tip strains were $\approx 50\%$. Strains in the near tip field were much more uniform and observations of interlamellar deformation were exceptional. However, the resolution of the AFM was not used on crack tips; rather photographs of the crack tip region made at 4000X were stereoimaged. An example of strain distribution determined at ambient temperature is shown in Figure 7. It was concluded that deformation at the higher strain amplitudes and fewer cycles at crack tips resulted in more homogeneous strains than deformation at lower strain for more cycles in a smooth initiation specimen.

Fatigue cracks were observed during crack growth studies in the SEM to blunt, grow, and sharpen in a manner similar to fatigue crack growth in aluminum alloys (18). Fatigue cracks growing perpendicular to the lamellar direction at intermediate ΔK interacted directly with the lamellae and crack extension appeared to by regulated by the lamellar structure. Cracks growing near ΔK_{th} were found to favor growth in the same direction as the lamellae and were stopped by colony boundaries.

The results from crack initiation and crack growth studies may be linked through the use of a model that treats fatigue crack growth as the failure of a small low-cycle fatigue specimen at the crack tip (19). From crack tip micromechanics and crack growth rate measurements, the slope (β) of the strain-cycle relation was determined, giving $\beta \approx -0.14$. Also the slope of the log stress vs. log cycles to failure (S-N) curve may be estimated from these results and the cyclic work hardening

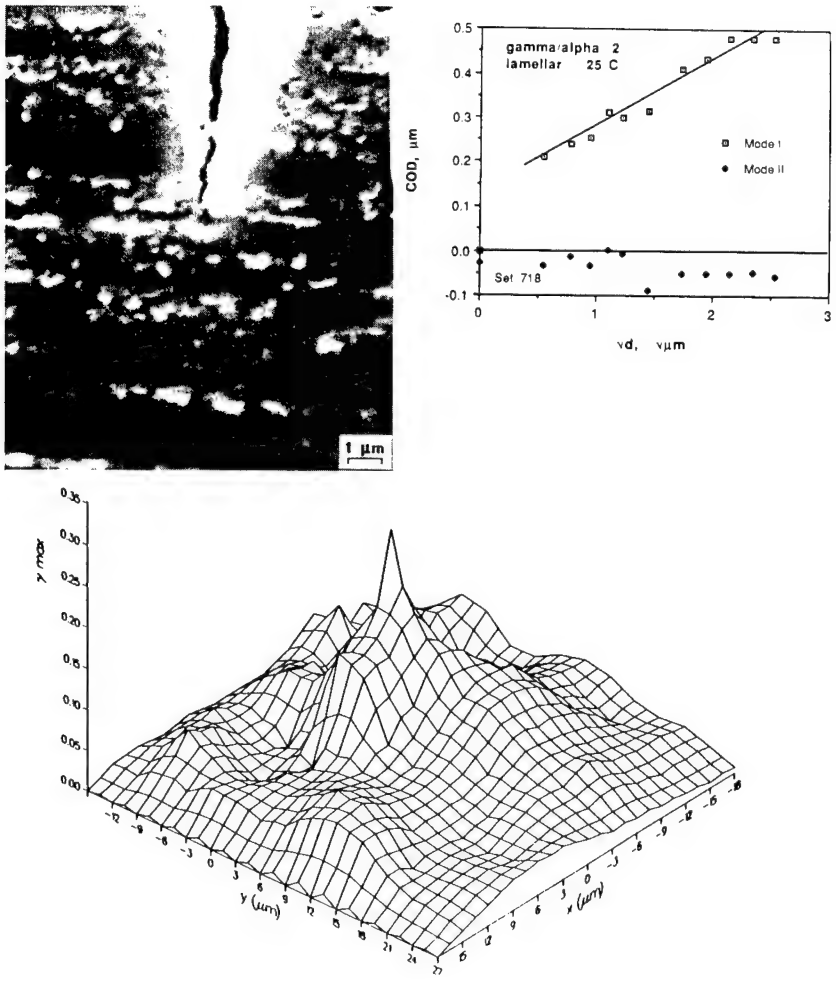

Figure 7. Crack opening displacement and distribution of maximum shear strain for a large fatigue crack growing perpendicular to the lamellae direction at $\Delta K = 23$ MPa$\sqrt{m}$. The crack tip is blunt, resulting in a large strain at the crack tip.

coefficient as $n' \approx -0.17$, which was approximately the same value as determined from the rotating beam experiments and agrees well with the results of Shih, *et al.* (18), and Dowling, *et al.* (20), for two-phase TiAl-alloys with either a lamellar or a duplex microstructure.

Compared to results for aluminum alloys, steels, and even other titanium alloys, the derived value of β, which is approximately -0.5 for those alloys, is very small; likewise the slope of the S-N curve is very shallow when compared to conventional materials. Confidence in the results comes because of the compatibility between all the values measured and derived.

Fracture Toughness

Two-phase TiAl-alloys with the lamellar microstructure are generally fairly resistant to crack growth under quasi-static tensile loading. Figure 8 shows the nonlinear load-displacement curve typically observed in J-testing of lamellar TiAl-alloys. Periodic unloading was made during J-testing in order to obtain the elastic compliance for crack extension measurements. The initial slope of the load-displacement is slightly nonlinear, indicating the presence of crack-tip plasticity

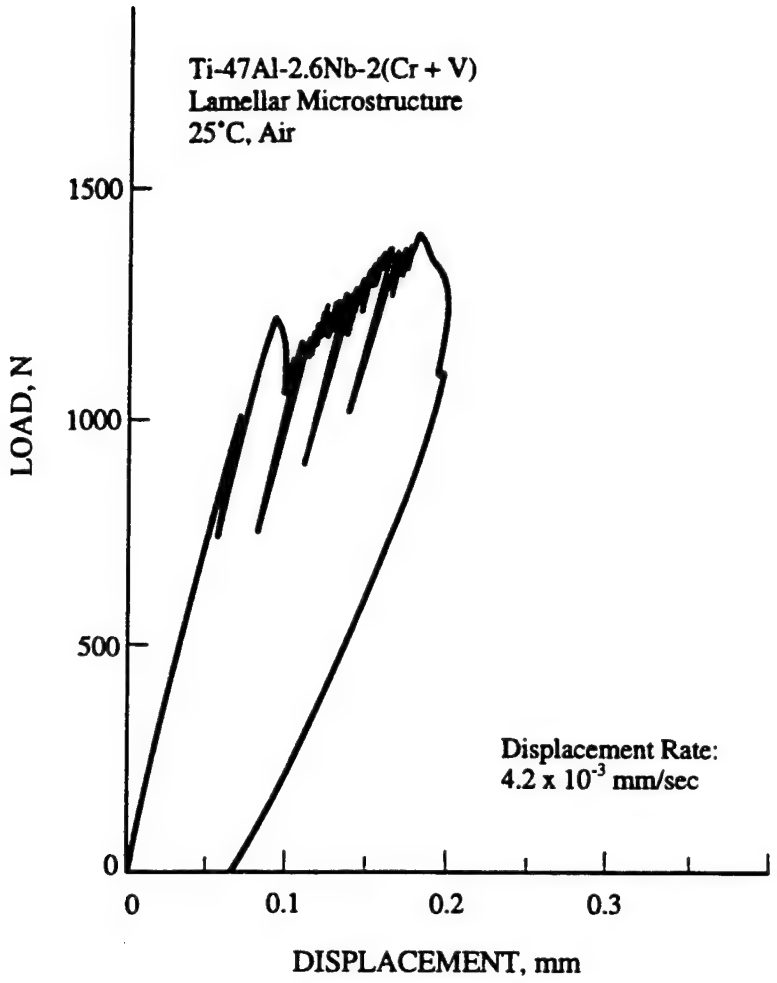

Figure 8. Typical load-displacement curve for the G1L alloy observed in J-testing.

or small amounts of near-tip microcracking. Initiation of crack growth is accompanied by a load drop. Further crack extension, however, requires increasing loads with increasing load-line displacements.

The fracture resistance of the lamellar alloy increases with increasing crack extension, leading to a fracture response that is best described in terms of a resistance-curve (4-6,10). Resistance-curve behavior has been observed in lamellar TiAl-alloys at 25°C and 800°C both in air and in vacuum (4-6,10,21-22). Figure 9(a) and (b) present resistance-curves of the G1L alloy tested in air for 25°C and 800°C, respectively. In these cases, the displacement rate varied from $1x10^{-4}$ mm/sec to $4.2x10^{-1}$ mm/sec. As indicated in Figure 9(a), initiation of crack growth in the lamellar TiAl-alloy tested at 25°C and $1x10^{-4}$ mm/sec commenced at K_{IC}=18 MPa$\sqrt{m}$. The K level required for subsequent crack growth increased in a diminishing rate with increasing crack extension, reaching a maximum at 33.5 MPa$\sqrt{m}$. Increasing the displacement rate led to only small changes in the K level where crack extension commenced. For example, the K_{IC} value was increased from 18 MPa$\sqrt{m}$ to 18.5, 20.9, and 22.5 MPa$\sqrt{m}$ when the displacement rate was increased from $1x10^{-4}$ mm/sec to $4.2x10^{-3}$, $4.2x10^{-2}$, and $4.2x10^{-1}$ mm/sec, respectively. Additionally, the resistance-curve behavior was only slightly altered by increasing the displacement rate. The maximum K value was either unchanged or was slightly increased by a higher displacement rate, Figure 9(a). At a given displacement rate, the resistance curve of the lamellar TiAl-alloy for 800°C is higher than that for 25°C. Unlike the results for 25°C, the entire

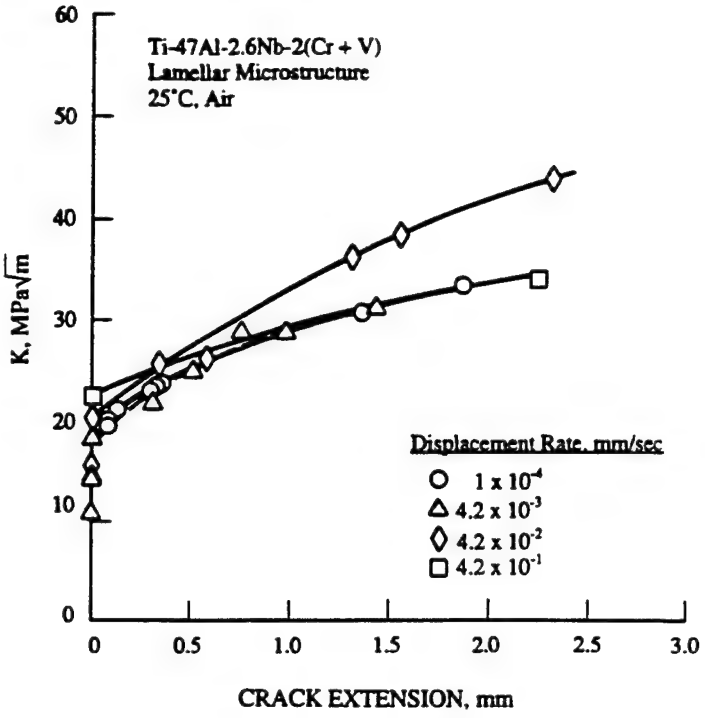

(a)

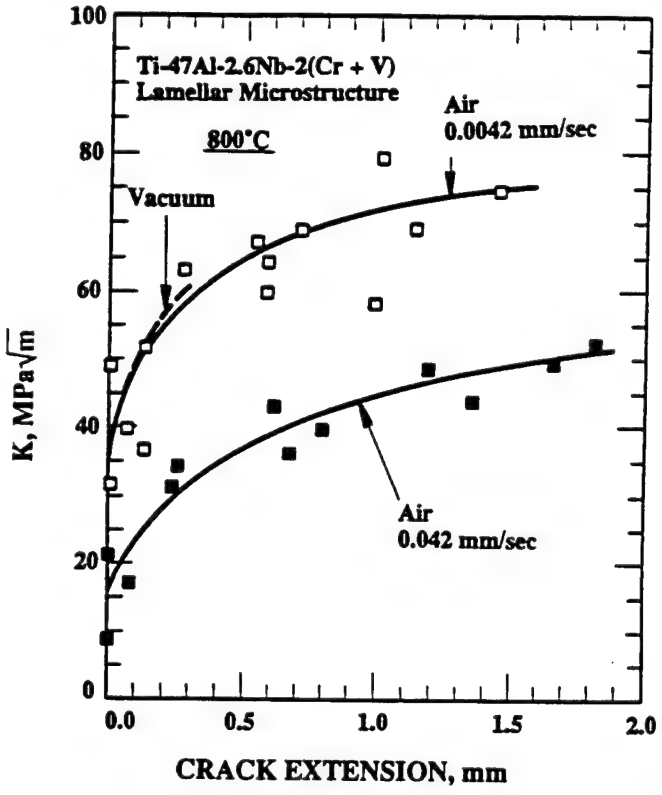

(b)

Figure 9. K-resistance curves for the G1L alloy at 25°C (a) and at 800°C (b).

resistance curve is reduced by an increasing displacement rate at 800°C, as shown in Figure 9(b). Thus, the fracture toughness of TiAl-alloys appears to be rate-insensitive at 25°C, but is rate-sensitive at 800°C.

The sources of crack growth toughness in lamellar TiAl-alloys are identical at 25°C and 800°C (4-6). In both cases, the resistance curve behavior arise from the formation of intact ligaments in the wake of the main crack due to either deflection of the crack path or the formation of unconnected, misaligned microcracks ahead of the tip of the main crack (4-6,10,21-22). The various means by which crack wake ligaments can be induced in lamellar TiAl-alloys are illustrated in Figure 10. Secondary colonies situated within a larger colony are one of the possible sources of crack-wake ligaments (10), Insert A in Figure 10. A common form of ligaments in lamellar TiAl-alloys is shown in Insert B in Figure 10; this ligament is produced by interface delamination of the lamellae on two parallel, unconnected planes within a single lamellar colony (4-6,21-22). Another commonly observed ligaments, shown in Figure 10, is formed when the main crack encounters or approaches a colony boundary. Frequently, microcracks are produced in an adjacent colony due to the stress or strain field of the approaching crack tip. The resulting microcrack, however, are generally misaligned with the main crack, primarily due to differences in crystallographic orientation in colonies containing the main crack and the microcrack (4-6,21-22). The ligament separating the main crack and the microcrack can be quite large, as illustrated by the region labeled C in Figure 10.

The stress state in the crack-wake ligaments are substantially different from that ahead of the tip of main crack. Fracture of the ligaments is usually, though not always, by shear (21-22) and involves propagating a crack normal to the lamellar interface, *i.e.*, translamellar fracture. As a result, translamellar slip or twining are frequently activated in the crack-wake ligaments. Fine translamellar slip in a crack-wake ligament is shown in Insert C in Figure 10. Note that translamellar slip or twinning requires a higher critical resolved shear stress than slip or twinning parallel to the lamellae (23). By instigating redundant deformation and fracture, the crack-wake ligaments improve the fracture resistance of the lamellar TiAl-alloys in a manner similar to ductile-phase ligaments (22). The fine translamellar slip shown in Figure 10 are observed mostly in crack-wake ligaments or near deflected crack tips, where shear stress are sufficiently high.

Discussion

One of the significant findings of in the recent studies of two-phase TiAl-alloys is that the lamellar microstructure is fairly resistant to crack growth under both monotonic and cyclic loads. In particular, translamellar fatigue or fracture with the crack growth direction being normal to the lamellae appears to be quite difficult. In contrast, fatigue or fracture in a direction parallel to the lamellar interface seems to be somewhat easier, resulting in a higher crack growth rate and probably a lower fracture toughness.

Another significant finding is that large cyclic strains could be attained at certain interlamellar regions. This is consistent with surface observations of extensive slip markings parallel to the lamellar interface. The slip markings and large cyclic strains were probably caused by slip in γ on slip planes that are parallel to the lamellar interface. The observation that extensive cyclic strain could occur without initiating microcracks either in γ or in the lamellar interface suggests that some of the lamellar interfaces are quite strong and resistant to crack initiation, even though crack initiation at or near the lamellar interface has been observed. These findings are consistent with previous observations that mating surfaces of low-energy fracture facets in lamellar

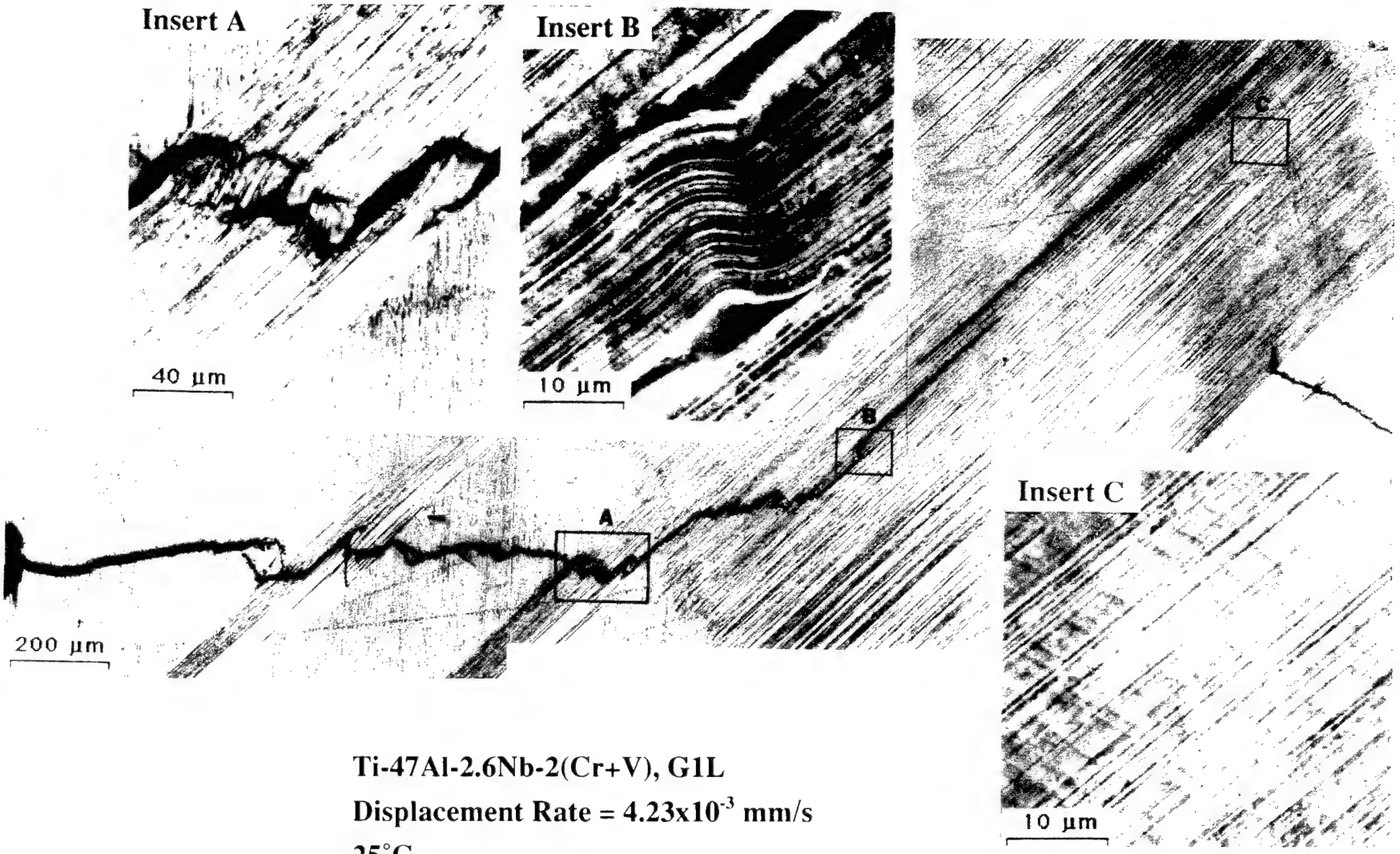

Figure 10. Profile of crack path in the G11 alloy with inserts showing secondary colony ligament (Insert A), misaligned crack planes and ligament (Insert B), and translamellar fine slip in a crack-wake ligament (Insert C).

alloys are usually of the γ / γ type, and less frequently the γ / α_2 type (13). At the present time, it is not understood why fatigue cracks initiated at the interlamellar region did not propagate when the crack size is small ($2a < 60$ μm).

For the displacement rates examined, the fracture toughness of the G1L alloy is rate-insensitive at 25°C, but is rate-sensitive at 800°C. Quantitatively, this fracture behavior resembles characteristics of thermally activated flow. It appears that deformation in the TiAl alloy is rate insensitive at 25°C, leading to crack tip deformation and K_{IC} values that are insensitive to the loading rate. At 800°C, deformation is thermally activated and rate-sensitive. A higher K_{IC} value is observed at a slow displacement rate because of extensive crack-tip deformation. As the displacement rate is increased, the crack-tip deformation is reduced and it leads to a lower fracture toughness value.

Despite the large local strains sustained at the crack-tip or at the interlamellar region, the lamellar alloys generally exhibit a relatively low tensile ductility whose value is on the order of 1-2% at ambient temperature (3-6). The seemingly contradictory results can be rationalized on the basis that microcracks are easily initiated in the lamellar microstructure under tensile straining. Once formed, these microcracks are capable of causing strain localization that is characteristic of an elastic-plastic crack. The result is that the nominal strain measured on the tensile specimen is generally quite low, despite large local strains sustained at the crack tip or in some interlamellar regions.

Conclusions

1. Tensile ductility of lamellar TiAl-alloys is rate-sensitive and is governed by the colony size and fracture resistance against propagation of microcracks that are initiated in the microstructure during tensile straining.

2. The local shear deformation caused by cyclic loading was remarkably large for this microstructure. Strains of up to 50% were derived by measuring the surface topography of cycled smooth specimens using atomic force microscopy. Strains of similar magnitude at the tips of large fatigue cracks were determined from displacements using stereoimaging.

3. The lamellar microstructure was remarkably resistant to the initiation of fatigue cracks. Stresses considerably in excess of yield were required to initiate cracks from pre-existing microstructural flaws, and these cracks would not continue growing unless the stress amplitude was increased.

4. Small fatigue cracks grew at ΔK values below the growth threshold for large fatigue cracks, ΔK_{th}, when small crack data for R=-1 are compared to large crack data for R=0.1.

5. The fatigue limit, which is the stress below which fatigue failure will not occur, is controlled by the nonpropagation of small cracks rather than by their initiation. The approximate level of the fatigue limit was 85% of ultimate tensile strength.

6. Large fatigue cracks growing perpendicular to the lamellae direction appeared to be controlled by lamellae width at high ΔK, while crack growing near ΔK_{th} preferentially grew parallel to the lamellae direction and were stopped by colony boundaries.

7. The slope of the cyclic stress strain curve was determined as n' = 0.17, the slope of the strain-life curve was derived from a model of crack growth as $\beta = -0.14$, and the slope of the S-N curve was derived from these factors. Data from the rotating beam specimens agreed with the derived slope of the S-N curve.

8. The relatively high fracture toughness in lamellar TiAl-alloys arises from a resistance-curve behavior instigated by crack-wake ligaments that are induced as the result of the formation of misaligned microcracks ahead of the main crack. Redundant deformation and fracture associated with fracture of the crack-wake ligaments leads to a relatively high crack growth toughness and the observed resistance-curve behavior.

9. The initiation toughness (K_{IC} value) of lamellar TiAl-alloys is rate-insensitive at 25°C, but is rate-sensitive at 800°C.

10. For a microstructure composed of two brittle intermetallic compounds, the lamellar microstructure is remarkably resistant to fatigue crack initiation and growth, and to quasi-static crack growth.

Acknowledgments

The authors are grateful for the support of this work by the Air Force Office of Scientific Research through Contract No. F49620-92-C-0022. The encouragement provided by the Program Monitor, Dr. Alan Rosenstein, throughout the course of this study is acknowledged. The authors are also thankful to Dr. Young-Won Kim at Universal Energy Systems for supplying the materials used in this study and discussion of this paper.

References

1. Y-W. Kim, *JOM*, 41 (7) (1989) 24-30.

2. Y-W. Kim and D. M. Dimiduk, *JOM*, 43 (8) (1991) 40-47.

3. Y-W. Kim, *Acta Metall. Mater.*, 40 (6) (1992) 1121-1134.

4. K. S. Chan and Y-W. Kim, Microstructure/Property Relationships in Titanium Aluminides and Titanium Alloys, ed. Y-W. Kim and R. R. Boyer (Warrendale, PA: TMS, 1991) 179-196.

5. K. S. Chan and Y-W. Kim, *Metallurgical Transactions A*, 23A (1992), 1663-1677.

6. K. S. Chan, *JOM*, 44 (5) (1992) 30-38.

7. S. L. Kampe, P. Sadler, D. E. Larsen, and L. Christodoulou, Microstructure/Property Relationships in Titanium Alloys and Titanium Aluminides, ed. Y.-W. Kim, R. R. Boyer, and J. A. Hall (Warrendale, PA: TMS, 1991) 313-322.

8. D. S. Shih, S-C. Huang, G. K. Scarr, H. Jang, and J. C. Chesnutt, Microstructure/Property Relationships in Titanium Aluminides and Alloys, (Warrendale, PA: TMS, 1991) 135-148.

9. W. O. Soboyejo, J. E. Deffeyes, and P. B. Aswath, *Material Science & Engineering*, A138 (1991) 95-101.

10. H. E. Deve, A. G. Evans, and D. S. Shih, *Acta Metallurgica et Materialia*, 40 (1992) 1259-1265.

11. D. L. Davidson and J. B. Campbell, *Metallurgical Transactions A*, (1993) in press.

12. D. L. Davidson, J. B. Campbell, B. K. Chapa, and J. Lankford, *Metallurgical Transactions A*, (1993) (submitted).

13. K. S. Chan and Y-W. Kim, *Metallurgical Transactions A*, 24A (1993) 113-125.

14. A. Nagy, J.B. Campbell, and D. L. Davidson, *Rev. Sci. Instrum.*, 55 (1992) 778-782.

15. D. R. Williams, D. L. Davidson, and J. Lankford, "Fatigue Crack Tip Plastic Strains by the Stereoimaging Technique," *Experimental Mechanics*, 20 (1980) 134-139.

16. E. A. Franke, D. J. Wenzel, and D. L. Davidson, "Measurement of Micro-Displacements by Machine Vision Photogramming (DISMAP)," Review of Scientific Instruments, 62 (5) (1990) 1270-1279.

17. D. L. Davidson and K. S. Chan, *Acta Metallurgica*, 37 (1989) 1089-1097.

18. D. L. Davidson and J. Lankford in High Strength Powder Metallurgy Aluminum Alloys-II, (Warrendale, PA: TMA, 1986) 47-57.

19. D. L. Davidson, *Acta Metallurgica*, 32 (1984) 707-714.

20. W. E. Dowling, Jr., B. D. Worth, J. E. Allison, and J. W. Jones, *Microstructure/Property Relationships in Titanium Aluminides and Alloys,* ed. Y-W. Kim and R. R. Boyer (Warrendale, PA: TMS, 1991) 123-134.

21. K. S. Chan, *Metallurgical Transactions A*, 22A (1991) 2021-2029.

22. K. S. Chan, *Metallurgical Transactions A*, 24A (1993) 569-583.

23. M. Yamaguchi, *Mat. Sci. Tech.*, 8 (1991) 299 - 307.

FRACTURE OF NIOBIUM CHROMIUM ALLOYS

FRACTURE OF NIOBIUM CHROMIUM ALLOYS

Introduction

Work has begun on evaluation of a series of niobium chromium alloys. The intermetallic compound of these elements, Cr_2Nb, has exhibited exceptional high temperature properties [1]: melting temperature is high (≈ 1700°C), and both creep resistance and oxidation resistance are exceptional at temperatures exceeding 1200°C. But, as with most intermetallics, Cr_2Nb is very brittle at ambient temperature. Alloying with additional Nb allows the formation of an "*in situ* composite" containing Cr_2Nb together with regions of Nb solid solution. As promising as this alloy/composite appears, evaluation of the fracture properties has not been undertaken. Our work on this system was begun this year, so only limited results have been obtained.

Design of Experiments and Production of Alloys

The addition of excess niobium creates a two phase material consisting of Cr_2Nb and a niobium solid solution phase, Nb(ss), that would be expected to behave in a more ductile manner than Cr_2Nb, so that the resulting material would exhibit increased ductility and fracture toughness. There should be a systematic increase in ductility and toughness as the fraction Nb(ss) phase is increased relative to the Cr_2Nb phase. Because the high temperature properties of this material depend on the characteristics of Cr_2Nb, there is likely to be a level of Nb(ss) that provides an optimum balance between ambient and high temperature properties. It is also possible that the morphology of the phases will affect the optimum ratio of phase and the levels of ductility and toughness. Several compositions of the binary alloys of Cr and Nb were chosen for characterization and evaluation of mechanical properties.

Four compositions of alloys were cast by United Technologies Research Center under the supervision of Dr. Donald Anton. The composition of these four materials and the resulting volume fraction of Cr_2Nb, as determined from the phase diagram, are shown in **Table 1**. It is well known that interstitial alloying additions greatly affect the properties of Nb based alloys; therefore, the interstitial content of these materials, measured after production, is included in the table. Interstitial level was not specifically controlled during casting, but resulted mainly from impurities in the starting materials.

Table 1

Composition of niobium chromium alloys

Alloy Designation	Niobium	Chromium	Cr_2Nb	Oxygen	Carbon
	at.%	at.%	%	%	%
012	55	45	66	0.013	0.025
013	59	41	57		
014	64	36	44	0.023	0.028
015	71	29	32	0.01	0.014

Hydrogen content was measured for alloys 012, 014 and 015 = 6 to 10 ppm.

After casting, each alloy was HIPed at 1500°C, 140 MPa, then heat treated at 1500°C for 8 hours. The resulting microstructure, which will be characterized further at a future time, consisted of irregularly shaped primary Cr_2Nb phase with regions of Nb(ss) in which an additional dispersion of small diameter, spheroidal, secondary Cr_2Nb was precipitated by the heat treatment.

Fracture Characteristics

Compact tension specimens approximately 20 mm square by 4 mm thick were cut from the castings of these four alloys using electro discharge machining (EDM). Each of the specimens was load cycled between compression and tension in order to initiate and grow a crack from the notch. Since the magnitudes of both the threshold for fatigue crack growth and fracture toughness of these alloys was unknown, great care was exercised in loading the specimens. Initially, load was cycled between a large value in compression and a small value in tension. As cycling continued beyond 10^5 cycles without crack initiation, the tensile load was gradually increased and the compression load decreased.

This procedure for inducing cracks produced initiation and growth of fatigue cracks from the notches of alloys 014 and 015, but resulted in broken specimens of the other two alloys, 012 and 013. The specimens that broke before cracks initiated from the notches fractured through the loading pin holes or from near the notch tip in the loading direction, i.e., perpendicular to the notch direction. These fractures indicated that the failure was caused by the large compression loads. The specimens probably broke because of tensile stresses that developed during the compressive loading part of the cycle.

The crack growth results obtained for materials 014 and 015 are shown in **Figure 1**. The data for material 014 was obtained from two specimens, while that for 015 was obtained from one specimen. Consequently, there is more scatter in the data for material 014. From these data, the fracture properties of these alloys have been estimated and are listed in **Table 2**. Constants are given for the crack growth relation

$$da/dN = B\Delta K^s \qquad (1)$$

Values of ΔK_{th} (the threshold stress intensity factor for fatigue crack growth) and K_c (the critical stress intensity factor, or fracture toughness value) derived from these data are also shown in the table.

Table 2

Fracture properties of Nb-Cr Materials

Material	B m/cycle	s	ΔK_{th} MPa$\sqrt{m}$	K_c MPa$\sqrt{m}$
014	7.5×10^{-24}	20	3.6	7.2
014 forged				7.9
015	2.8×10^{-52}	64	4.15	5.3

Threshold (ΔK_{th}) was defined for a crack growth of 10^{-12} m/cycle, and K_c was defined for 10^{-6} m/cycle. With the large scatter in the data for material 014, a range of values for the parameters in Table 2 is possible: $3.2x10^{-21} < B < 1.9x10^{-24}$ m/cycle, $15 < s < 27$, $3.4 < \Delta K_{th} < 3.8$ MPa$\sqrt{m}$, and $6.4 < K_c < 8$ MPa$\sqrt{m}$.

One piece of 014 material was forged at 1500°C, approximately 50 % reduction, then heat treated for 8 hrs. at 1500°C, all in argon atmosphere. A chevron notched specimen of this material was tested in bending, giving the fracture toughness value shown in the table. A CT type specimen was made also, but it broke during the crack initiation phase of testing in a manner similar to that described above for 012 and 013 materials.

From these limited data, no firm conclusions can be made, other than these *in situ* composites are relatively brittle and exhibit little damage tolerance. However, Cr_2Nb is reported to have a toughness of only ≈ 2-3 MPa$\sqrt{m}$, so there is some enhancement, perhaps a factor of 2.5 to 4, in toughness due to formation of the composite with Nb(ss). The reason that material 015, which has the most Nb(ss) is less tough and has a steeper crack growth rate curve than material 014 is not known at this time. The result was expected to be the opposite. It could be hypothesized that differences in the morphology of the Nb(ss) are the cause, but that possibility requires further exploration.

Reference

1. D.L. Anton and D.M. Shah "High Temperature Properties of Refractory Intermetallics" in **High Temperature Ordered Intermetallic Alloys IV**, J.A. Johnson, et al., eds., Mat. Res. Soc. vol 213, 1991, pp. 733-738.

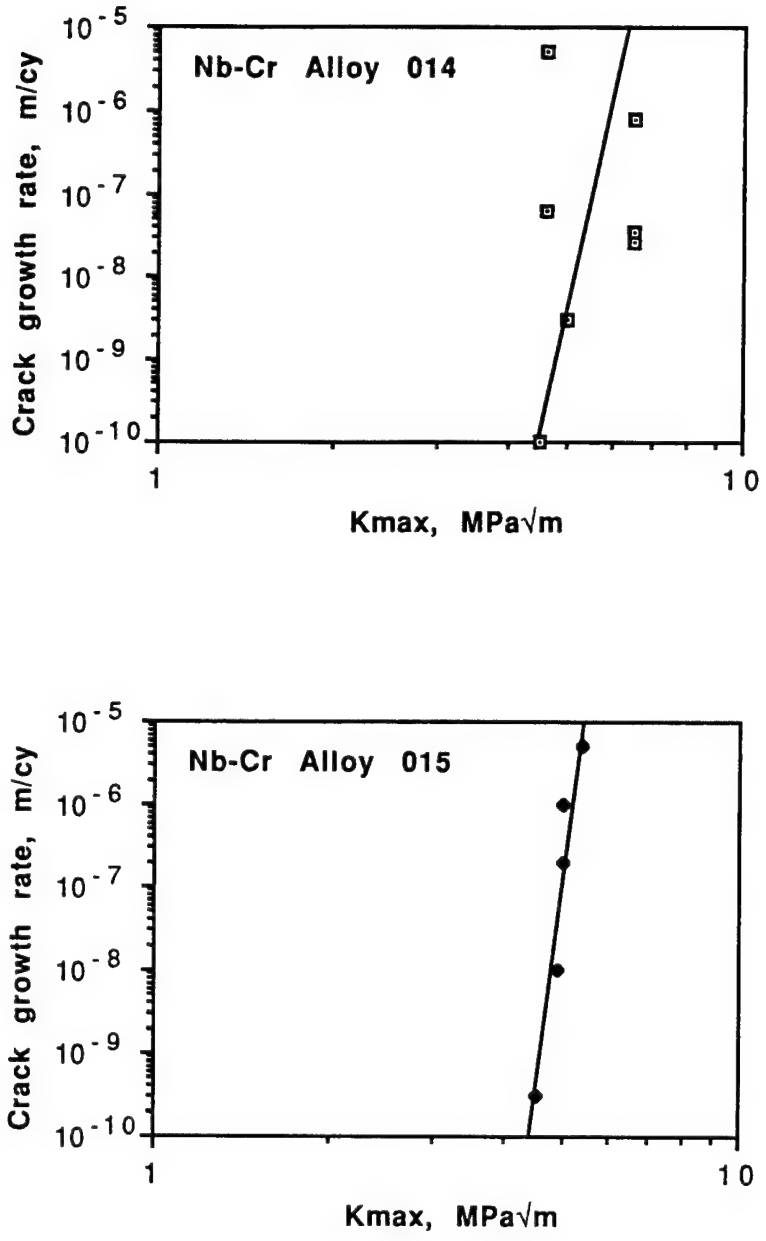

Figure 1 Fatigue crack growth rates for Nb-Cr alloys

INTERPRETATION OF RESULTS

INTERPRETATION OF RESULTS

For the Ti-Al based lamellar alloys, sufficient fatigue crack growth information now exists within this research program to warrant further interpretation. The fatigue characteristics of a number of titanium based alloys were compared and interpreted [1], and this analysis is now extended to include the lamellar TiAl alloys.

Some background is required to understand the analysis. It is only given in sketch form here, with reference to the more complete analyses. Models have been developed that couple the crack opening displacement and strain in the plastic zone of the fatigue crack tip to the cyclic stress-strain curve, and these models use the strain-life fatigue law as a failure criterion. There have been a large number of models developed with these assumptions, and they have been reviewed as a group, indicating their similarities, differences, and the assumptions inherent in each [2].

Only the model derived by Davidson [3] will be used to indicate how the various fatigue parameters fit together, but this model has many similarities to other models [2]. The physics incorporated in this model is based on considering the geometry of the crack tip, otherwise, the approach is mainly empirical.

The following parameters are measured and used in the analysis:

Cyclic stress-strain:	$\Delta\sigma = K_1(\Delta\varepsilon_p)^{n'}$	(1)
Strain-life relation:	$\Delta\varepsilon_p \Delta N^{\beta} = \varepsilon_c$	(2)
Crack tip strain:	$\Delta\varepsilon_p(0) = K_0 \Delta K_{eff}^{r}$	(3)
Crack growth rate:	$da/dN = B'\Delta K_{eff}^{s'}$	(4)

For crack tip strain and crack growth rate, ΔK_{eff} is used as the correlating parameter. Because of closure measurements on many alloys, including many of the titanium alloys, it is possible to easily determine ΔK_{eff} using the relationship

$$\Delta K_{eff} = \Delta K - \Delta K_{th} \qquad (5)$$

and with this relationship, the parameters B' and s' in the modified crack growth relationship given by equation (5) may be derived.

The crack growth model attributes crack opening displacement to dislocations being generated at the crack tip and moving into the plastic zone on slip lines. The model allows the parameters describing crack growth (B' and s') to be directly related to the crack tip parameters describing material failure (b and e_c). The following relationships may be derived [3]:

$$s' = (n'+1/\beta)/r \approx 1/\beta r$$
$$n = n'r$$

Thus, slope s' of the da/dN-ΔK_{eff} curve is related to the slope of the strain-life curve b, and r, the increase in strain with increasing ΔK_{eff}, and to minor extent, n', the cyclic work hardening rate. These correlations indicate that the parameter **r** is an important variable, but one for which there is presently no continuum mechanics model. These equations have been used with measured values of **r** to derive

parameters describing material at the crack tip (β and ε_c). These parameters are given in Table 1[1].

Table 1

Fatigue Crack Parameters for titanium alloys

Material	r	β	ε_c	s'	Ductile v_f
TiAl	0.37	0.17	0.15	2.2	0.01
Ti-14Al-21Nb	0.73	0.55	0.18	2	0.25
Super α2	1.0	0.57	0.28	1.8	0.50
Ti-6Al-4V	1.9	0.77	0.47	3.1	0.74
CORONA-5	1.1	0.64	0.66	1.8	0.85

The volume fraction of ductile phase for the alloys other than TiAl was measured, and that has been explained [1]. However, in lamellar TiAl alloy it is much more difficult to derive the amount of "ductile phase." The value given in the table is a very rough estimate based on the concept that most of the deformation occurs within 4 Burgers vectors of the lamellar boundaries. This was derived from the cyclic deformation and fatigue crack growth results that were summarized in an earlier section of this report. From the widths of the lamellae and the distance between (111), an estimate of the level of "ductile phase" volume of 0.01 was made.

The hypothesis has been made that the fatigue properties vary with the level of ductile phase [1]. This hypothesis is not new, having been used to explain the ductility of two phase alloys. For a recent summary of approach, see Fan and Miodownik [4].

How the parameters in **Table 1** change with fraction of ductile phase is shown in **Fig. 1**. For some parameters, there appears to be a smooth and systematic change, but for other parameters there is significant scatter. The poorest correlation, in comparison with other alloys, is for Ti-6Al-4V. The reason for this is not known, but it should be noted that this is the first titanium alloy on which the model was used 10 years ago, so these results may not be as accurate as for the other alloys. For the trends indicated, it is not important to know the exact volume fraction of "ductile phase" in the TiAl alloys, only that it is small, and that is easily justified.

Because of limited data, not much interpretation of the effects of *in-situ* composite formation on the fracture of Nb-Cr alloys can be given at this time.. However, the fatigue crack growth parameters thus far obtained can be compared with those of the titanium alloys on the basis of the amount of ductile phase present. In making this comparison, shown in **Fig. 2**, the amount of ductile phase has been chosen as being very small (0.001 for material 014), and 015 was assigned twice that of 014 because of the higher content of Nb(ss). Based on cursory fractography of materials 014 and 015, this assumption might be reasonable, but more work remains.

The comparison of crack growth parameters is made on a log-log basis so that all the materials can be included. On the basis of the comparison with titanium alloys, B' for 015 appears to be anomalous and the crack growth rate exponent s' for both alloys appears to be $\approx$ 5 times larger than expected. Thus, the Nb-Cr alloys do not seem to fit with the correlations derived for the other intermetallic alloys studied, e.g., those based on TiAl and Ti_3Al.

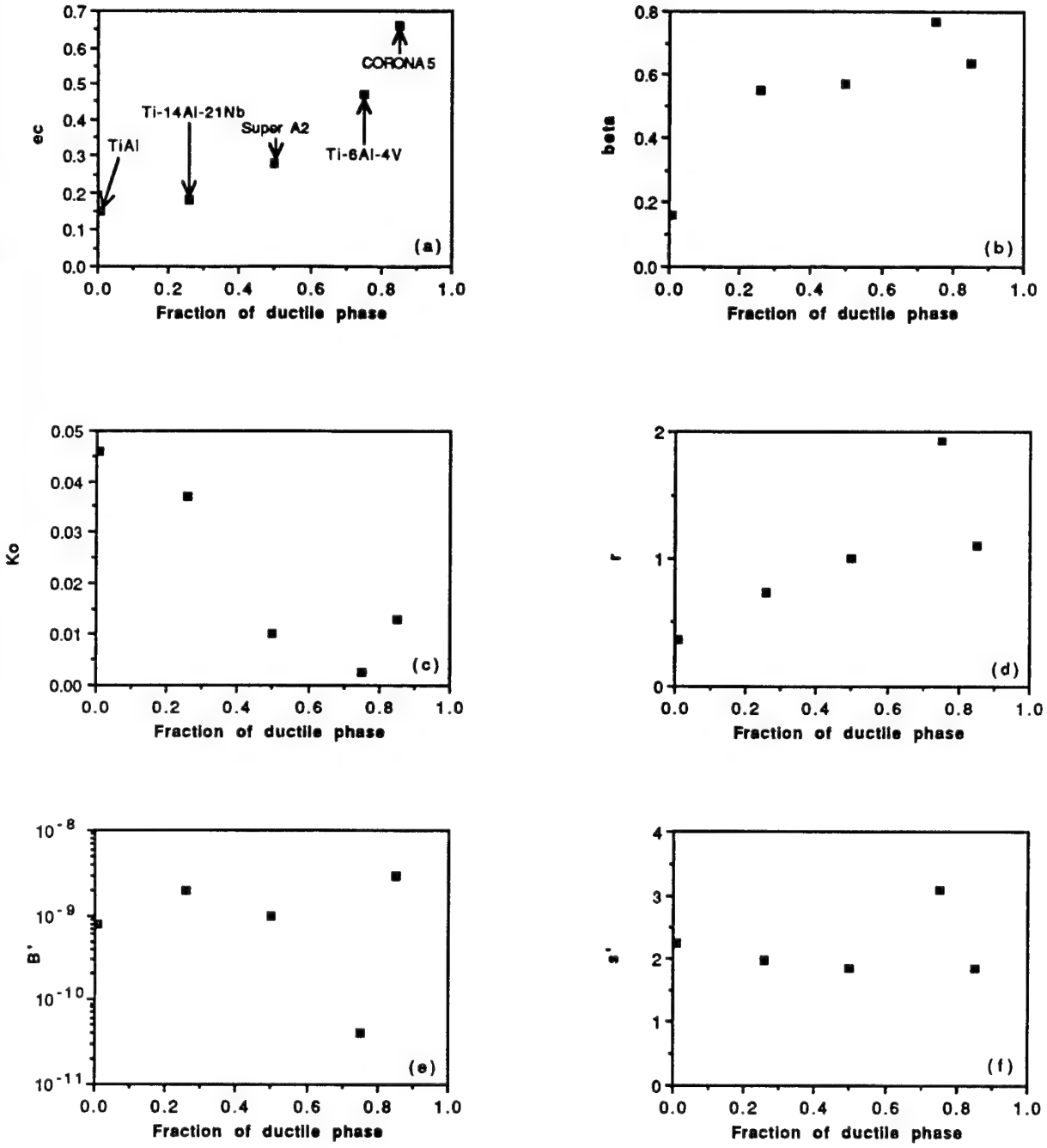

Figure 1 Variation of parameters that describe fatigue crack growth with the volume fraction of ductile phase in titanium alloys

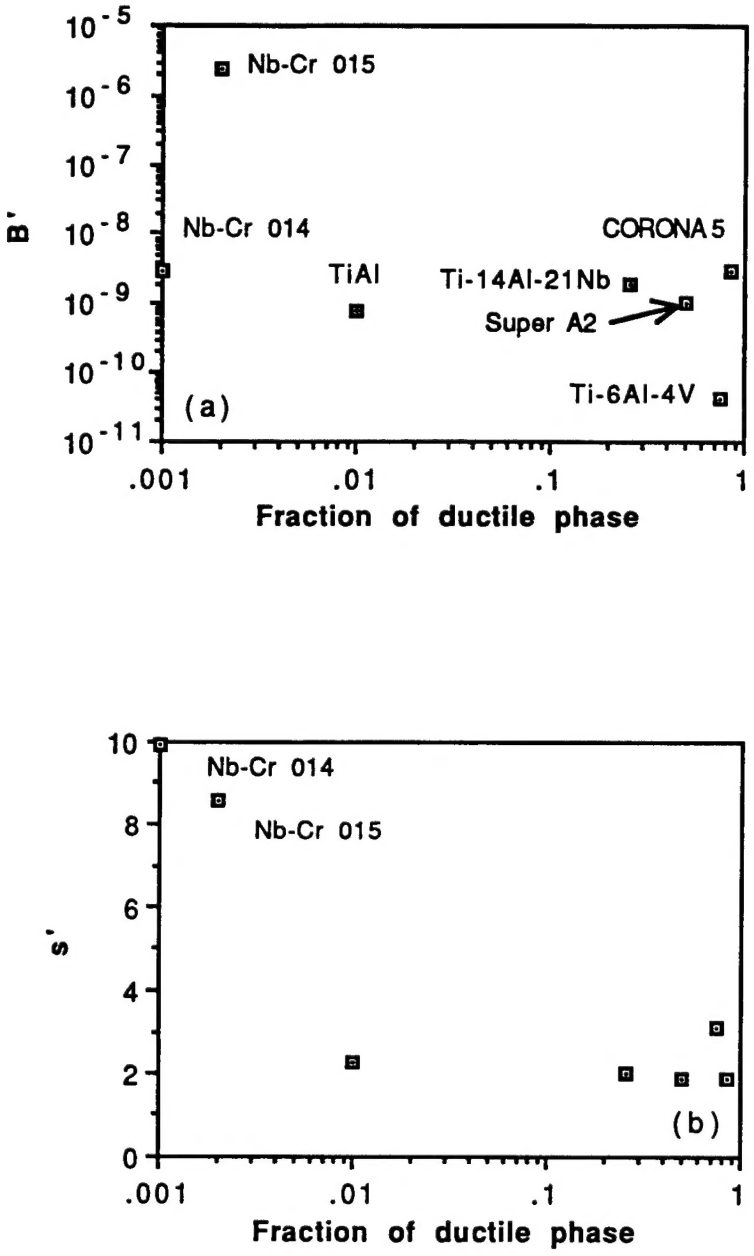

Figure 2 Comparison of the parameters in $da/dN = B'\Delta K_{eff}^{s'}$ with the amount of ductile phase for titanium and Nb-Cr alloys.

References

1. D.L. Davidson, "Titanium alloys: fatigue crack growth mechanisms and crack tip micromechanics" in **Microstructure/Property Relationships in Titanium Aluminides and Alloys**, Y-W. Kim, et al., eds, TMS, 1991, pp. 447-461.

2. D.L. Davidson and J. Lankford, *Inter. Materials Revs.*, 1992, v. 37, pp. 45-76.

3. D.L. Davidson, *Acta Metall.*, 1984, v. 32, pp. 707-714.

4. Z. Fan and A.P. Miodownik, *Script Metall et Mater.*, 1993, v. 28, pp. 895-900.

PUBLICATIONS

PUBLICATIONS

1. "Fatigue and Fracture in Lamellar TiAl Alloys," K. S. Chan and D. L. Davidson, **International Symposium on Structural Intermetallics**, Seven Springs Meeting, September 1993 (submitted).

2. "Cyclic Plasticity and Small Fatigue Crack Growth in a TiAl-Based Alloy with a Lamellar Microstructure," D. L. Davidson, J. B. Campbell, B. K. Chapa, and J. Lankford, *Met. Trans. A*, 1993 (in review).

3. "Fatigue Crack Growth Through the Lamellar Microstructure of an Alloy Based on TiAl at 25 and 800°C," D. L. Davidson and J. B. Campbell, *Met. Trans. A*, 1993 (in press).

4. "Influence of Microstructure on Crack-Tip Micromechanics and Fracture Behaviors of a Two-Phase TiAl-Alloy," K. S. Chan and Y-W. Kim, *Met. Trans. A*, Vol. 23A, 1992, pp. 1663-1677.

5. "Rate and Environmental Effects on Fracture of a Two-Phase TiAl-Alloy," K. S. Chan and Y-W. Kim, *Met. Trans. A*, Vol. 24A, 1993, pp. 113-125.

6. "Understanding Fracture Toughness in Gamma TiA," K. S. Chan, *JOM*, Vol. 44, No. 5, May 1992, pp. 30-38.

7. "Toughening Mechanisms in Titanium Aluminides," K. S. Chan, *Met. Trans. A.*, Vol. 24A, 1993, pp. 569-583.

8. "Fatigue and Fracture in Lamellar TiAl Alloys," K. S. Chan and D. L. Davidson, **Proceedings of the International Symposium on Structural Intermetallics**, Campion, PA, 1993 (in press).